Materials & Design 254 (2025) 114075

Contents lists available at ScienceDirect

Materials & Design

journal homepage: www.elsevier.com/locate/matdes

The potential microbial inactivation mechanisms of reduced graphene oxide functionalized textiles

Qinghong Huang [a], Tianyu Kou [a], Mingrui Liao [b], Tianhao Ge [b], Jing Liu [a], Jian R. Lu [b], Heng Zhai [c,*], Yi Li [a,*]

[a] Department of Materials, The University of Manchester, Manchester M13 9PL, UK
[b] Department of Physics & Astronomy, The University of Manchester, Manchester M13 9PL, UK
[c] Department of Chemical Engineering, The University of Manchester, Manchester M13 9PL, UK

ARTICLE INFO

Keywords:
Photothermal effect
Cotton fabric
Reduced graphene oxide
Antimicrobial ability
Reduced graphene oxide yarn

ABSTRACT

Disinfection is crucial for medical protective clothing (MPC), as improper disinfection may cause secondary transmission during use and after disposal, especially for reusable MPC (RMPC). Reduced graphene oxide (rGO), a photosensitive material, has the potential to kill microorganisms by generating heat or voltage on textiles. To investigate this, we tested both photothermal and photovoltaic effects of rGO coated canionised (Cat-rGO) cotton fabric and the wet spinning rGO yarn with the xenon lamp, and a series of physical properties were also tested. Results show that under sufficient light intensities, Cat-rGO fabric easily reaches temperatures that can kill various common viruses, evidently inactivate both *Escherichia coli* and *Staphylococcus aureus*, and dries faster than pristine fabric. For rGO yarn, its temperature is significantly lower than Cat-rGO fabric when attached on common cotton fabric. As for photovoltaic effect, however, only rGO yarn can generate a voltage under light exposure, while Cat-rGO fabric does not. Despite this, in general, using the photothermal effect of Cat-rGO fabric to kill microorganism is more effective. This study demonstrates that Cat-rGO fabric can disinfect using light alone, without chemicals, metals, or extra equipment. It is an ideal choice for self-disinfecting RMPC and for use in medical facilities.

1. Introduction

The COVID-19 pandemic has resulted in a disaster worldwide without exception [1], and the importance of personal protective equipment (PPE) has been highlighted [2,3]. Medical protective clothing (MPC) is a typical type of textile PPE, which can be divided into disposable MPC (DMPC) and reusable MPC (RMPC). The pollution caused by disposable products has raised serious concerns in society [4,5], and the pollution from disposable PPE has also been a severe problem during the pandemic [6]. Compared with using DMPC, RMPC can save much water, energy and materials, and reduce solid waste [7]. A main function of MPC is to prevent pathogens from entering the human body, and viruses are one of the major targets of it. Viruses degrade more quickly on soft, water-absorbing surfaces than on hard, water-resistant surfaces [8,9]. This is because water-absorbing materials will promote liquid spread within their structure, accelerating evaporation, which in turn impacts virus survival. [9,10]. Meanwhile, because the liquid remains within the fibrous structure rather than being repelled from the surface, water-absorbing textile products can reduce droplet and aerosol transmissions, which are two typical transmission routes of respiratory viruses. However, many viruses can still survive on dry surface for days [8,11–16].

To provide RMPC with better protection for the human body, and to avoid secondary transmission, disinfection is a key consideration [17]. Widely used disinfection methods for PPE include chemical disinfectants (such as ethanol), heating, hydrogen peroxide vapor, and ultraviolet radiation [17,18]. For conductive textile product, electricity is also used to disinfect [19], which kills bacteria and viruses through electroporation of their membrane [20–22]. Another method is adding antimicrobial materials into textiles [23,24]. Some typical antimicrobial metals, such as zinc, copper, and silver [25–27], have been widely used for killing microorganisms in the textile product. Organic chemicals have

Abbreviations: Cat, Cationised; Cat-rGO, Cationised and Reduced Graphene Oxide Coated; DMPC, Disposal Medical Protective Clothing; GO, Graphene Oxide; MPC, Medical Protective Clothing; rGO, Reduced Graphene Oxide; RMPC, Reusable Medical Protective Clothing; WCA, Water Contact Angle.

* Corresponding authors.
E-mail addresses: heng.zhai@manchester.ac.uk (H. Zhai), henry.yili@manchester.ac.uk (Y. Li).

https://doi.org/10.1016/j.matdes.2025.114075
Received 27 January 2025; Received in revised form 5 April 2025; Accepted 6 May 2025
Available online 7 May 2025

also been used for antimicrobial protection [28,29]. In comparison to chemical disinfectants and antimicrobial materials, using high temperature inactivation has no chemical hazards or environmental pollution. Furthermore, compared to using professional equipment and rooms to generate a high temperature, raising the temperature of textile products with light energy can reduce equipment and space dependence, and help save power consumption.

Many types of viruses can become inactive at 56 °C [30–38], and HPIV can even be inactivated at 50 °C within 15 mins [39,40]. Previous studies have demonstrated that laser-induced graphene can be added to face masks, with its photothermal ability to kill bacteria and viruses by high temperature [41,42]. Graphene and its derivatives have many special physical and chemical properties, such as photocatalytic ability, high conductivity, high surface-to-volume ratios and antimicrobial ability [43–45]. Therefore, they have long been among the top choices for medical and biological materials [46–48]. RGO is a popular choice for photothermal materials [49,50]: Liu et al. demonstrated that chitosan/rGO cotton fabric absorbs light from 200 to 2500 nm [51]. Zhao et al. added reduced graphene oxide-zinc-aluminum hydroxide to nylon fabric [52], which could increase the fabric temperature by about 40 °C under exposure to a xenon lamp light source. Also, if there is a temperature difference within conductive or semiconductive materials, these materials can generate an electromotive force; this phenomenon is called the thermoelectric effect. When the temperature difference is triggered by light exposure, it can also be viewed as the photovoltaic effect. Meanwhile, because rGO is conductive and can generate heat, it is also possible to generate a voltage in the textile products [53], equipping them with potential for virus disinfection. Viruses can be killed by anodic oxidation. For instance, COVID-19 can be inactivated by voltage of 5 V within 5 mins [54], and Bacteriophage MS2 can be inactivated by 3.5 V within 24 mins [55].

RGO can be coated onto textile products by first coating with graphene oxide (GO), and then reducing it [51]. Graphene-based materials can form hydrogen bonds with cotton fibres [56], and be coated onto textile products through simple pad mangle dyeing [56,57]. The cotton fabric is woven from cotton yarns, and each yarn is twisted from numerous cotton fibres. Cotton can become cationic through reaction with cationic agents [58], and 3-chloro-2-hydroxypropyl trimethyl ammonium chloride (CHPTAC) is one such agent [59,60]. GO is anionic [43], so cationic cotton can capture more GO and allow GO to attach more strongly to the cotton [61,62]. Additionally, GO can be used in wet spinning to make fibres [63], which can be twisted into yarns [64], and then be reduced to rGO yarn in a subsequent procedure [64]. L-ascorbic acid can reduce GO to rGO at warm temperature [65,66], which is more environmentally friendly than reducing GO with hazardous chemicals or high temperatures [57,67].

In this study, different physical properties of rGO coated cationised (Cat-rGO) fabric and rGO yarn are tested. For comparison, 5 other types of cotton fabric samples are also tested: pristine white fabric, cationised (Cat) fabric, black fabric, GO coated fabric, and the rGO coated fabric. Meanwhile, antibacterial testing of fabric samples is conducted to investigate the potential antimicrobial ability of Cat-RGO fabric. The results reveal that cationised cotton fabric captures more rGO than pristine cotton fabric, and the performances of Cat-rGO fabric in terms of water resistance and photothermal effect are better than those of rGO fabric. Under the same light source, Cat-rGO fabric reaches a higher temperature and dries faster than black fabric. Moreover, Cat-rGO fabric exhibits clear antibacterial ability to both Gram-negative bacteria (*E. coli*) and Gram-positive bacteria (*S. aureus*), especially to *E. coli*. The rGO yarn presents good conductivity and exhibits both photothermal and photovoltaic effects. Overall, the photothermal effect is better than the photosensitive effect in killing microorganism.

2. Experiment

2.1. Materials

CHPTAC (60 wt% in H_2O), expandable graphite flakes, L-ascorbic acid (≥99%), Sodium chloride and Tween 20 were purchased from Sigma-Aldrich. Ethanol absolute, sodium hydroxide, and acetic acid were purchased from VWR Chemicals. Potassium permanganate (>99%) was purchased from Acros Organics. Sulfuric acid (≥95%), hydrogen peroxide (>30% w/v) and hydrogen chloride (32%) were purchased from Fisher Chemical. Remazol Black B gran 133 % (Remazol B) was purchased from Dystar. Sodium carbonate was purchased from Fluka, Honeywell. Fibrecrafts Synthrapol was purchased from Georgeweil. The substrate fabric used in this experiment is 100% cotton, suitable for casual wear, which can be found in our previous research. [68].

2.2. Surface-modified cotton fabrics

The cotton fabric was prewashed in absolute ethanol solution to remove impurities and referred to as pristine fabric. A black cotton fabric was fabricated to compare with the rGO coated cotton fabrics. The GO ink was prepared under modified Hummers' method as shown in our previous study [64]. To achieve a firmly bonded structure between rGO and cotton fabrics, a cationized cotton fabric (Cat fabric) was firstly prepared. The rGO fabric and Cat-rGO fabric were fabricated by pad dyeing rGO onto pristine fabric and Cat fabric respectively. The fabrication procedures were described in Fig. S1 (Supporting Information).

2.3. Fabrication of rGO yarns

The fabrication of rGO yarns was conducted following our previous research [64]. Fig. S1f illustrates the formation of a continuous GO fibre in a rotating stand. The GO dope was extruded through a 0.4 mm diameter spinneret to form a GO fibre through a solidification process in a coagulation bath. The GO fibre was then wound in 30 loops of the same diameter in the bath. After incomplete removal of coagulation solution, the partially-damp fibre loops were cut at the same length and manually twisted into a single GO yarn. The rGO yarn was prepared after a reduction process.

2.4. Characterization

The optical images were captured under the D65 light from a light booth (Multilight, Datacolor). The micro images were captured by scanning electron microscopy (Sigma, Zeiss). The light transmittance and reflectance were measured by UV/Vis/NIR Spectrophotometer (Lambda 1050, PerkinElmer). The thickness of the synthetic GO was measured by Atomic Force Microscopes (AFM) (Multimode8, Bruker), and the used probe is SCOUT 350 RAI, NuNano. Raman spectroscopy was performed using LabRAM (Evolution HR, Horiba) with a 633 nm laser. X-ray photoelectron spectroscopy (XPS) was conducted using Axis Ultra (Kratos), utilizing monochromatized Al Kα radiation, and the spot size of the X-ray was approximately 700 × 300 μm. The water contact angle was tested using a Drop Shape Analyzer (DSA 100, Kruss) with deionised (DI) water.

2.5. Photosensitive effect

The photothermal effect was studied by a xenon lamp (PLS-SXE300+/UV, Perfectlight): Fabrics were cut as disc samples of 3.8 cm in diameter. When testing rGO yarn, the yarn was fixed on the pristine fabric with white cotton yarns. Fabric and rGO yarn samples were placed in the lab (20 ± 1 °C) for 24 h before testing. Three disc samples of each kind of fabric and three rGO yarn samples were tested once. Four kinds of light source were used: UV, green, red, and visible light. The light source was changed by using different kinds of lamp filter. A metal wire

holder was used to keep the samples approximately 5 cm above the table surface. The irradiances of light sources were measured using a solar power meter (Solar-100, Beha-Amprobe). The fabric's temperature was monitored using infrared camera (C3 1.2, Flir). This camera can show the temperature of samples' central round area, and the round area can be seen in IR images.

The fabric drying time under different light sources was studied as followed: 100 μl of DI water was dipped and evenly spread on the fabric disc for 1 min, then the damped sample was exposed to different light sources using the same method. The infrared camera was used to monitor the water drying process. Similarly, three disc samples of each kind of fabric were tested once. The time counting started when the lamp was switched on, and stopped just before the sample's temperature started dramatically rising.

The photovoltaic effect was studied by a multimeter (2000, Keithley): As shown in Fig. S2, the edge of the disc sample was clamped with crocodile clips, and the rGO yarn was fixed with hook clips. The fixed length of the rGO yarn was 4 cm. Clips were attached to a small platform, which could be moved left and right by turning the handle. Before the light exposure, the resistances of disc samples and rGO yarn were tested. During the light exposure, the disc sample or rGO yarn was regularly moved, and the voltage change was monitored by the multimeter. Three samples were tested for each kind of fabric or yarn, and each sample was tested once.

2.6. Antibacterial experiment

The antibacterial experiment refers to International Standard BS EN ISO 20743 (2021). Bacteria used here are *Escherichia coli* (ATCC 25922) and *Staphylococcus aureus* (ATCC 6538). The antibacterial ability was tested as followed: Firstly, the fabric disc samples were exposed under UV light for about 30 mins before using for sterilising. 10 μL of bacteria solution with OD_{600} w = 0.2 was dipped onto the centre of each sample and fully spread. The dampened sample was placed onto a Petri dish, and the dish was put on the metal holder under the xenon lamp. The sample was exposed to the light for 5 mins in the fume hood, and its temperature was monitored with infrared camera. The control group was placed in the biosafety cabinet after the solution was dipped. Two different methods were used to transfer bacteria from fabric samples to agar plates: the method one involved attaching the fabric disc to the agar plate well for 30 min, then the disc was gently peeled off. 10 μL phosphate-buffered saline (PBS) solution was added for lubrication and the cell spreader was used to spread the bacteria evenly over the plate. The plates were incubated for 18 to 24 h. This method was repeated once. In the method two, the disc samples were immersed in 12 ml of PBS solution for 30 mins. The following procedures were the same as in the previous study [26], and 10 μL liquid from the original gradient to 1000 times dilution gradient was dropped onto the agar plates. The plates were incubated for 18 to 24 h.

3. Result and discussion

3.1. The optical and surface properties

To cationise the pristine fabric, CHPTAC was first converted to 2,3-epoxypropyl trimethylammonium chloride (EPTAC) in a NaOH solution, enabling it to react with the cellulose in cotton fibres (Fig. 1**a**). This process facilitates the coating of GO onto fabric due to the attraction of cationic cotton to the anionic GO [61,62], as shown in Fig. 1**b and c**, and the hydrogen bond also help capture GO [56]. The AFM image in Fig. 1**d** displays the GO flake obtained from the GO solution, with a thickness of approximately 1 nm, which is the characteristic of single-layered GO [69]. This thickness allows the GO flakes to form a nanometer-thin film on the cotton fibers.

Fabric colour directly affects the light absorption rate of fabric. The optical images of different fabric samples and their colour values in the CIELAB colour space are shown in Fig. 2**a & b**, and Table S1. L ranges from black (0) to white (100), A ranges from green (negative) to red (positive), and B ranges from blue (negative) to yellow (positive). The colour on squares in Fig. 2**a** was added using Photoshop, and these colour values are derived from Table S1. The results show that colours of the pristine and Cat fabric are similar, and they appear quite white. The black fabric has the deepest colour, with a slight blue tint. The GO fabric is slightly yellow and darker than the pristine and Cat fabric. The A and B values of the rGO and Cat-rGO fabrics show no clear bias; they are darker than the GO fabric but lighter than the black fabric. Meanwhile, the colour of Cat-rGO cotton is deeper than that of rGO cotton. This phenomenon can be explained by the rGO content: the colour of rGO is dark green, as the content of rGO increases, the colour of the coated fabric also becomes deeper. This phenomenon reveals that CHPTAC enhanced the cotton fabric's ability to capture GO.

The micro-sized differences in surface morphology among fabric samples can be viewed in SEM images (Fig. 2**c**, Fig. S3 and Fig. S4). Compared with the image of pristine fabric, the black dyeing and cationization with CHPTAC have no visible effect on the surface and shape of cotton fibres. SEM images of GO, rGO and Cat-rGO fabrics show that

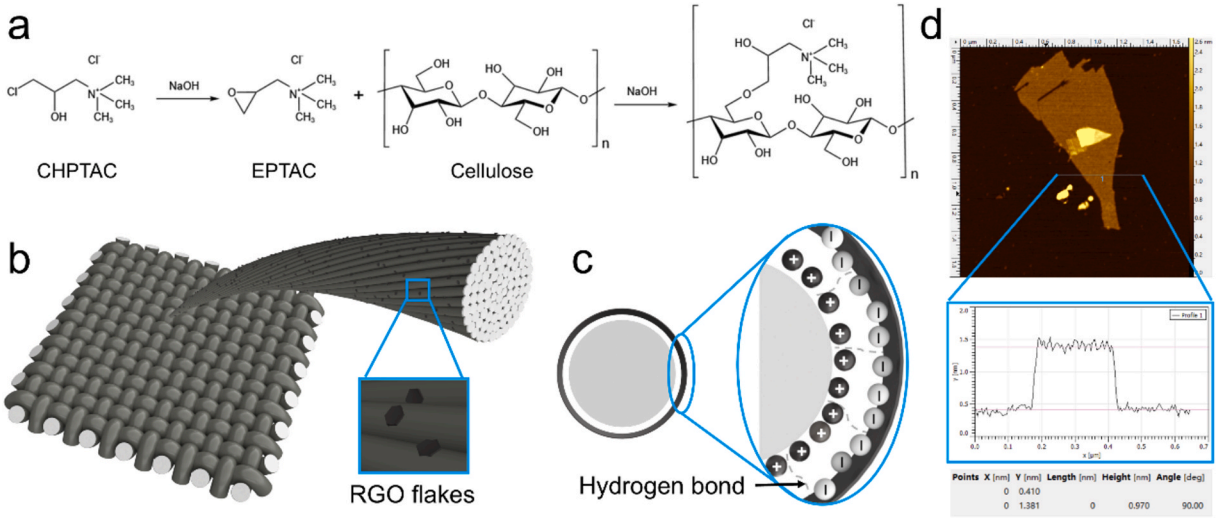

Fig. 1. a) The chemical reaction of CHPTAC and cellulose. **b)** The structure of rGO coated cotton fabric. **c)** The mechanism of coating rGO onto the surface of cotton fibre. d) AFM image of the GO flake from the GO solution and its measured thickness.

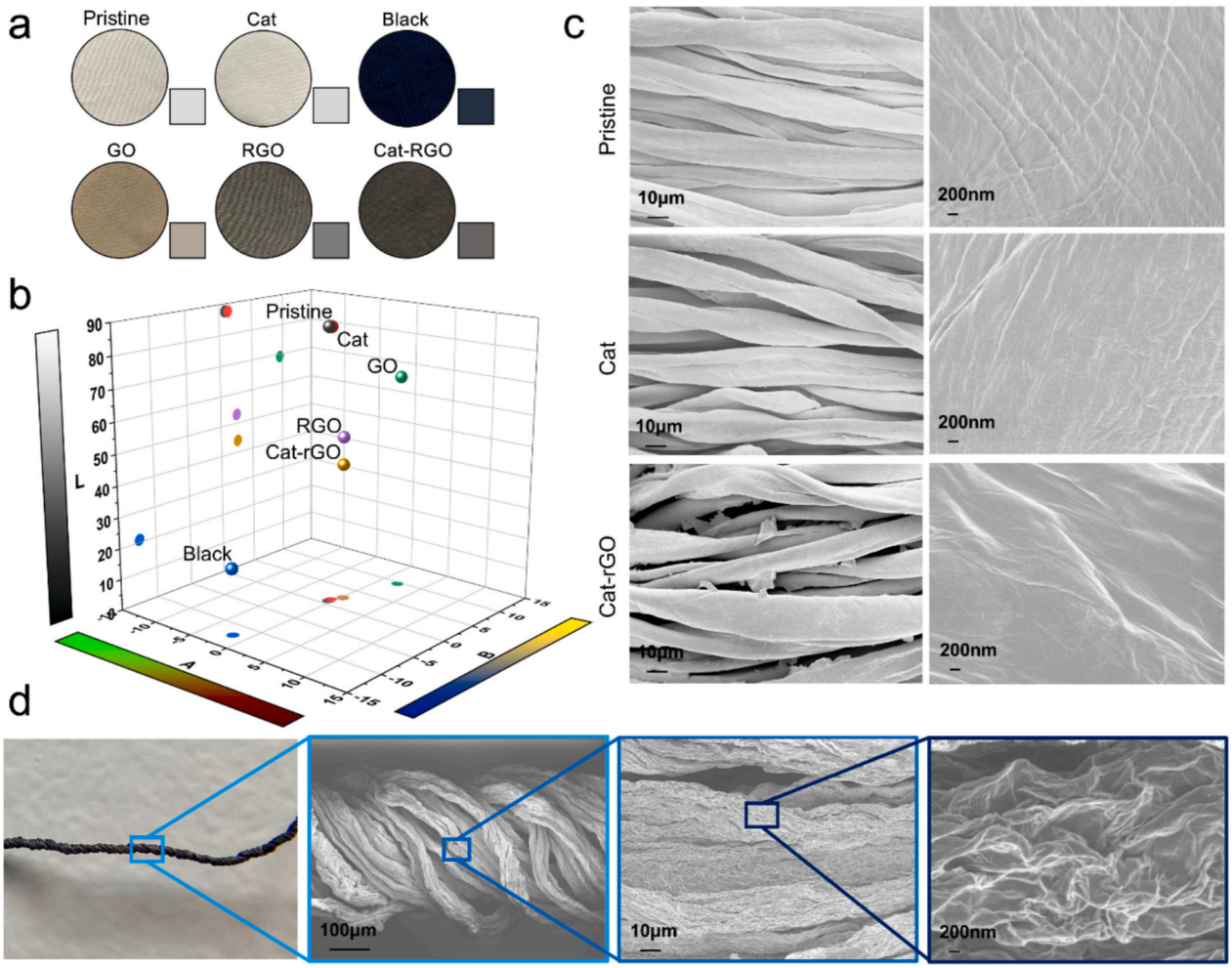

Fig. 2. A) The colour of different fabric samples and their squares of mean value colours. **b)** The positions of different fabric samples in CIELAB colour space. **c)** The SEM images of different fabric samples. **d)** The rGO yarn's optical images (left) and SEM images of different magnifying ratio (the others).

GO and rGO flakes were homogeneously coated on the surface of cotton fibres. Additionally, SEM images with higher magnification reveal that compared with the pristine, Cat and black fabrics, GO and rGO also form a thin membrane on the fibre surface of GO, rGO and Cat-rGO fabric. RGO yarn presents a deep colour and uneven structure on a macro scale, as shown in Fig. 2**d**. The thickness of rGO yarn is around 0.4 mm. The microstructure and surface morphology of rGO fibres can be seen in SEM images of Fig. 2**d**, where rGO fibres were twisted together, and there are small gaps among them. The shape of rGO fibres is irregular, and their surface is rough, which was formed during the fibre drying process.

3.2. *The characterization of different fabrics and RGO yarn*

The existence of GO and rGO are reflected by the Raman spectra of the fabric samples and RGO yarn (Fig. 3**a**). Each fabric type's intensity ratio between the D peak and G peak (I_D/I_G) are added to the graph, which were calculated from three testing results of each kind of fabric. The G peak is the main characteristic peak of graphene [70], and the D peak represents the defect level of GO and rGO [71]. I_D/I_G reflects the disorder level of GO and rGO [70]. After reduction, the ratio between the intensities of the D peak and G peak increased visibly [65], which is caused by the decrease in the size of sp^2 domains [57,67]. I_D/I_G of Cat-rGO is higher, which may be caused by the electrostatic force between CHPTAC and rGO increasing the defect level of rGO [72]. RGO yarn has a significantly higher I_D/I_G compared with rGO fabric, as it underwent deeper reduction with hydroiodic acid.

The content of GO and rGO can be reflected by XPS results of different fabric samples and RGO yarn: The C/O ratio of GO fabric is higher than that of pristine fabric, but not by much, which is because the C/O ratio of GO is close to that of pristine cotton fabric [73,74]. The C/O ratio of rGO is higher than that of GO, and it increases as the reduction degree deepens [65]. Each fabric type's atomic percentage ratio between carbon and oxygen (C/O ratio) are added to Fig. 3**b**, which were calculated from three testing results. Hence, the C/O ratio of rGO fabric is higher than that of GO fabric. When the rGO content increases, the C/O ratio increases. In contrast, CHPTAC and Remazol B have a smaller influence on the ratio of carbon and oxygen, as the content of both chemicals on the fabric is too low. The C/O ratio of rGO yarn is far higher than Cat-rGO, because it is made of pure rGO.

Because the differences in the surface morphology, the light transmittance and reflection rates of fabric samples are also different, as shown in Fig. 3**c and d**. As cotton fabrics aren't transparent, the transmittance rate of all fabric samples to light is lower than 1%. Therefore, the reflection rate dominates the light absorption. The pristine, Cat, black and GO fabrics have similar reflection rates for light with wavelengths greater than 1500 nm. Moreover, the overall reflection rates of pristine and Cat cotton are similar; they reflect nearly 100% of visible light and absorb some UV light. GO fabric reflects less light with wavelengths below 1250 nm; black fabric has the lowest reflection rate for light with wavelengths below 700 nm. The reflection rate of rGO fabrics for all wavelengths of light is lower than 30%, and the reflection rate of Cat-rGO fabric is consistently lower than 20%.

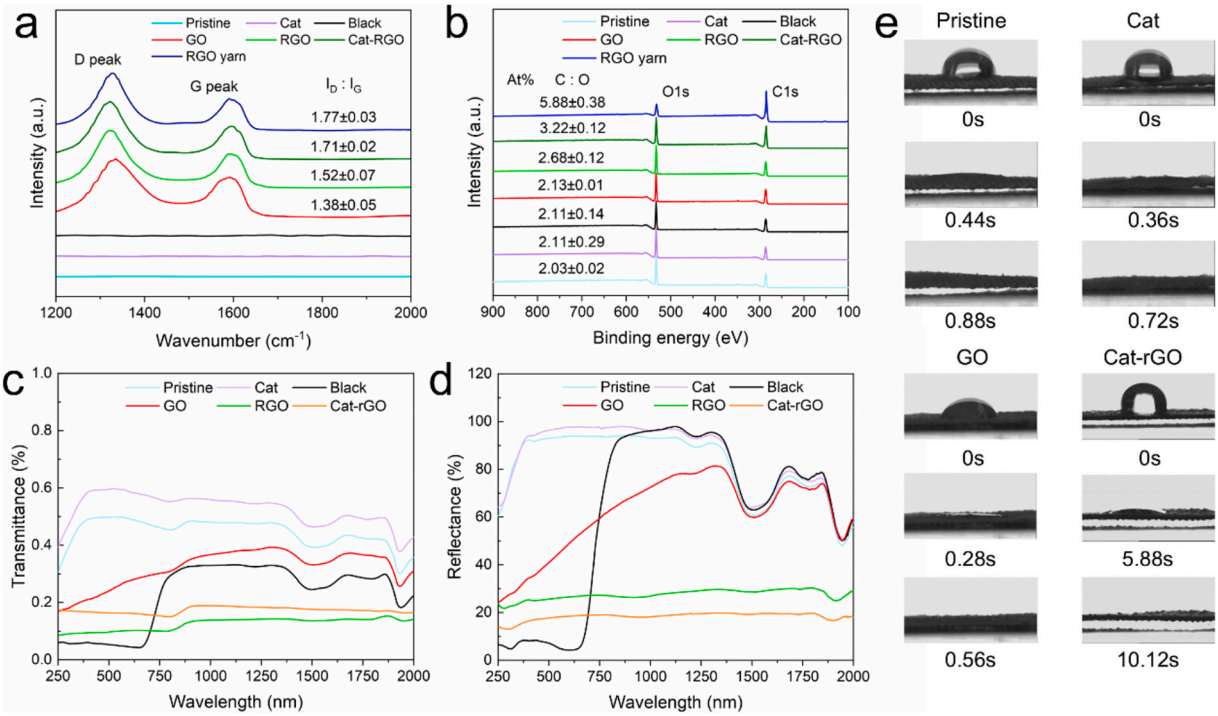

Fig. 3. **a)** Raman spectra of different fabric samples and rGO yarn. **b)** XPS spectra of different fabric samples. **c)** The transmittance to light of different fabric samples. **d)** The reflectance to light of different fabric samples. **e)** The dynamic water contact angles of different fabric samples.

The changes of water resistance are reflected by the dynamic water contact angle of different fabric samples (Fig. 3**e** and Fig. S5). The times indicated on the images below of Fig. 3**e** and Fig. S5 represent when each image was captured. Each fabric sample's mean value and standard deviation of damping times calculated from three testing results. The damping times of Cat fabric (0.61 ± 0.08 s) and black fabric (0.83 ± 0.10 s) are shorter than those of pristine fabric (1.07 ± 0.16 s), which may be caused by the hydrophilicity of CHPTAC and Remazol B. The damping time of GO fabric (0.51 ± 0.08 s) is the shortest, as GO has hydrophilic properties and its content level is high enough [75]. RGO has the hydrophobic property [76], therefore the damping time of rGO fabric (3.89 ± 0.99 s) is significantly longer than that of pristine fabric. Cat-rGO fabric contains more rGO than rGO fabric, so even though it contains CHPTAC, its damping time (9.33 ± 1.35 s) is the longest, more than twice as long as rGO fabric. As mentioned in the introduction, viruses degrade more quickly on soft, water-absorbing surfaces [8,9], and water-absorbing textiles can reduce droplet and aerosol transmissions. Therefore, Cat-rGO fabric maintains a reasonable water absorption for MPC.

3.3. *The photothermal effect of rGO coated fabrics*

The testing method of photothermal effect is displayed in Fig. 4**a** and Fig. S2. When using the UV, green, and red light, the fabric samples were placed under the xenon lamp at a distance of 10 cm from the light source. As the visible light has a wider wavelength range, it has stronger power. When using the visible light, the lamp was placed 40 cm away from the fabric sample. The light spectrum of the xenon lamp and the performance parameters of different lamp filters are shown in Fig. 4**b** and Table S2, and the irradiances of different light sources are shown in Table S3. The filters of UV, green, and red light will only let UV, green, and red light, respectively, to pass through, while the filter for visible light was a UV cutoff filter, which blocked light with a wavelength shorter than 420 nm but allowed other light to pass through. Fig. 4**c** shows the 4 light types used in the experiment.

Many viruses can still survive on dry surface for days, as shown in Fig. 4**d** and Table S4. Meanwhile, many types of viruses can become inactive at 56 °C As shown in Fig. 4**e** and Table S5. Fig. 4**f** shows the detected temperature of fabric samples. Cat-rGO fabric can reach 56 °C regardless of the type of light used. RGO fabric can reach 56 °C with green, red, and visible light. For the other fabrics, only the black fabric can reach 56 °C when visible light is used. Fig. S6 shows the temperature increase of different fabric samples under different light sources compared with the room temperature (20.7 °C). As shown in Fig. 4**b**, the green light has the highest intensity, followed by red light, with UV light having the lowest intensity. Therefore, among UV, green, and red light, the temperature increase under green light is always the highest, and the temperature under UV light is the lowest. The wavelength of lamp's visible light ranges from 420 nm to 1000 nm. Hence, visible light has the greatest power to increase the fabric temperature. For rGO yarn, as it is only a single yarn, although it increases the temperature of the pristine fabric, its temperature is far lower than that of rGO fabric and Cat-rGO fabric under all four kinds of light sources.

Among all kinds of fabric samples, regardless of the light source used, the temperature increase of pristine fabric and Cat fabric is the lowest. Cat fabric's temperature increases are similar to that of pristine fabric, indicating that CHPTAC didn't visibly affect the photothermal ability. GO fabric's temperature is higher than that of pristine and Cat fabric, but lower than that of black fabric. This phenomenon indicates that GO has no intrinsic photothermal ability on the cotton fabric; it relies on its deeper colour to absorb more light and increase the temperature. Under UV, green, and red light, rGO and Cat-rGO fabrics reach higher temperatures than black fabric, which shows that rGO triggers its photothermal effect upon light exposure, and the photothermal effect can be triggered by light of any wavelength. Meanwhile, because Cat-rGO cotton has more rGO than rGO cotton, its temperature is higher than that of rGO cotton. When fabric discs are exposed to visible light, the influence of fabric colour becomes more important, so the black fabric's temperature increase is higher than that of rGO fabric. As Cat-rGO fabric has a deeper colour than rGO fabric and contains more rGO, the temperature increase of Cat-rGO fabric is still the highest.

As Cat-rGO has the strongest photothermal effect, it was chosen for

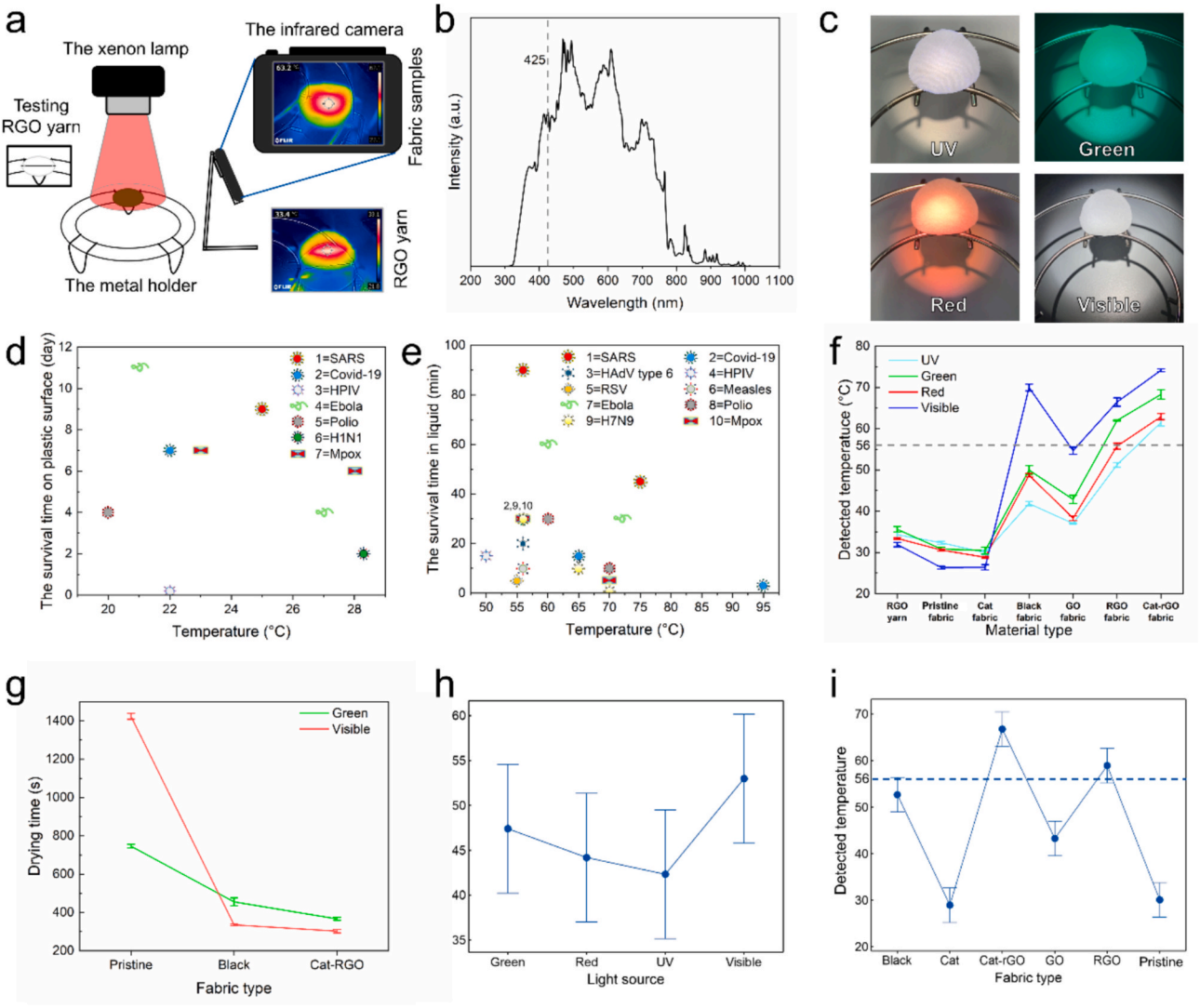

Fig. 4. a) The testing method of the photothermal effect of fabrics and rGO yarn. b) The light intensity spectra of the xenon lamp. c) The four light types used in the experiment. The inactivation temperature and time of some typical viruses in different environment: d) When viruses are on the dry plastic surface (1: SARS [11], 2: Covid-19 [8], 3: HPIV [12], 4:Ebola [13], 5: Polio [14], 6: H1N1 [15], 77: Mpox [16]). e) When viruses are in a liquid environment (1: SARS [30], 2: Covid-19 [31], 3: HADV type 6 [32], 4: HPIV [39,40], 5: RSV [33], 6: Measles [34], 7: Ebola [35], 8: Polio [36], 9: H7N9 [37], 10: Mpox [38]). The photothermal effect of rGO yarns and fabrics: f) The temperature of different kinds of fabric and rGO yarn under different light sources. The 56°C dash line indicates the lowest temperature for inactivating viruses. g) The drying time of fabric samples under green or visible light. h) The interval plot of detected temperature vs light .
Source. i) The interval plot of detected temperature vs fabric type. The 56 °C dash line indicates the lowest temperature for inactivating viruses

further comparison with the pristine and black cotton. Meanwhile, as green light can increase the temperature more than red and UV light, it was chosen to be used alongside visible light. Fig. 4**g** shows the drying times of damp fabrics under green or visible light. Under both green and visible light, Cat-rGO dries in the shortest time, further proving that the photothermal effect of rGO performs better than deep colour. Besides, compared with green light, both black and Cat-rGO fabrics dry quicker under visible light, which proves that the higher temperature can dry the fabric faster. The pristine fabric takes the longest time to dry, and the drying time under visible light is much longer than under green light. The reason can be explained by the uniform distribution of visible light on the fabric discs. As shown in Fig. 4**c**, when using visible light, the distance between the lamp and the fabric disc is greater than when using UV, green and red light, so the visible light spreads more evenly on the fabric disc. For the other three light sources, their central points have a higher irradiance, so the fabric's centre has a higher temperature compared to its edge during exposure. As the pristine and Cat fabric reflect most of the light over 500 nm, their central temperature becomes the lowest under visible light, as shown in Fig. 4**f**. Therefore, the drying time of dampened pristine fabric under visible light is much longer than under the green light.

Minitab was used to investigate the influence of fabric type and light source on the detected temperature of fabric, and ANOVA general linear model was selected. As the fabric has 6 types (pristine, Cat, black, GO, rGO and Cat-rGO fabric) and there are 4 kinds of light sources, the fabric type has 6 levels, and the light sources have 4 levels. Fig. S7 shows the calculation result. The model fits the data well with a coefficient of determination of 90.92%. The result shows that both light source and fabric type have a significant impact on the temperature ($P < 0.0005$), with fabric type having a greater impact than the light source, as it has a higher F-value of 116.52. Fig. 4**h** is the interval plot of detected temperature of fabric vs. light source. The mean value with 95 % CI of visible light is distinct from the other three light sources, and the differences among the other three light sources are relatively small. Fig. 4**i** is the interval plot of detected temperature vs. fabric type. The mean values with 95% CI of pristine and Cat fabrics are similar, but the

differences between them and other fabric types, as well as the differences among other fabric types, are obvious. Therefore, the fabric type has a bigger effect on the detected temperature.

In general, Cat-rGO fabric exhibits better performance than rGO yarn in the photothermal effect, and it also performs better than the black fabric. Besides, its generated temperature is high enough to inactivate viruses.

3.4. The photovoltaic effect of rGO yarn and rGO coated fabrics

The testing method of photovoltaic effect is displayed in Fig. 5**a** and Fig. S2. The resistance of the fabric disc was calculated by the detected overall resistance dividing its area (3.8 cm radius), and the resistance of rGO yarn was calculated by the detected overall resistance dividing its length (4 cm). As shown in Fig. 5**b** and Table S6, the overall resistance of rGO fabric is out of multimeter's range (over $1*10^{37}$ Ω), so it is considered as an insulator. Cat-rGO fabric is conductive, although its resistance is over $2*10^5$ Ω/cm^2, and the overall resistance of its disc is over $3*10^6$ Ω. For rGO yarn, the resistance is only (218 ± 7) Ω/cm, and the overall resistance of its sample is less than 1000 Ω.

The generated voltage values are shown in Fig. 5**c**&**d** and Table S6. Fig. 5**c** shows the generated voltage when the highest light irradiance is at the left end of the yarn and fabric, while Fig. 5**d** shows the generated voltage when the highest light irradiance is at the right end of yarn and fabric. As shown in Fig. 5**e**, when the light irradiance is the highest at one end of the yarn, the yarn will generate the highest voltage; when the light irradiance is the highest at the other end, the yarn will also generate the highest voltage but in the opposite direction; when the light irradiance is spread evenly on the yarn, it will not generate voltage. As shown in Fig. S8, the generated voltage had a limited impact on the resistance of rGO yarn: the resistance decreased by less than 5% when a voltage was generated. For fabrics, unexpectedly, under both green and visible light, rGO and Cat-rGO fabric didn't generate any voltage, regardless of their position under the lamp. Fig. 5**c**&**d** show the highest voltage generated by rGO yarn is about 65 μ V, which is far lower than the required level to kill bacteria or viruses [54,55].

Three factors may explain why the Cat-rGO fabric didn't generate voltage: The first factor is the high overall resistance of the fabric disc, as a medium with high resistance will loss most of the voltage it transmits. The second factor is that, as rGO spreads evenly over the surface of the cotton fabric, it integrates as a two-dimensional surface. Compared to the one-dimensional rGO yarn, it is harder to create a temperature difference within the surface when exposed to light. The third factor is the distribution of rGO on the cotton surface is relatively even, so the structure and density differences of rGO among different areas are small, making it harder to produce a potential difference. For rGO yarn, its structure is quite uneven, as it is twisted by dozens of rGO fibres. This uneven structure results in a greater difference within rGO yarn during light exposure.

Minitab was used again to investigate the influence of light position and light source on the detected voltage of rGO yarn, and ANOVA general linear model was selected. The light position was divided into two levels (left and right), and the light source was divided into two levels (green and visible). Fig. S9 shows the calculation result. Both light position and light source impact the generated voltage of rGO yarn ($P < 0.05$), and the light source has a more significant impact ($P < 0.0005$). Fig. 5**f** shows the interval plots of voltage vs. light source and light position. As mentioned in section 3.3, the light irradiance of visible light is more even than that of green light. Therefore, the temperature difference on the rGO yarn generated by visible light is smaller than generated by green light. That is the reason why the generated voltage is significantly lower under the green light. The light position has a relatively small difference, and this difference may be caused by the uneven thickness and structure of the rGO yarn.

In general, rGO yarn exhibits better performance than rGO coated fabric in the photovoltaic effect, but its generated voltage is still too low to inactivate bacteria and viruses.

3.5. The antibacterial performance of different fabric samples

As visible light has the strongest intensity and is more uniform than other single-wavelength light, it was chosen for the antibacterial experiment. The antibacterial experiment procedure, which is described in section 2.3.3, is displayed in Fig. 6**a**. The temperature of fume hood

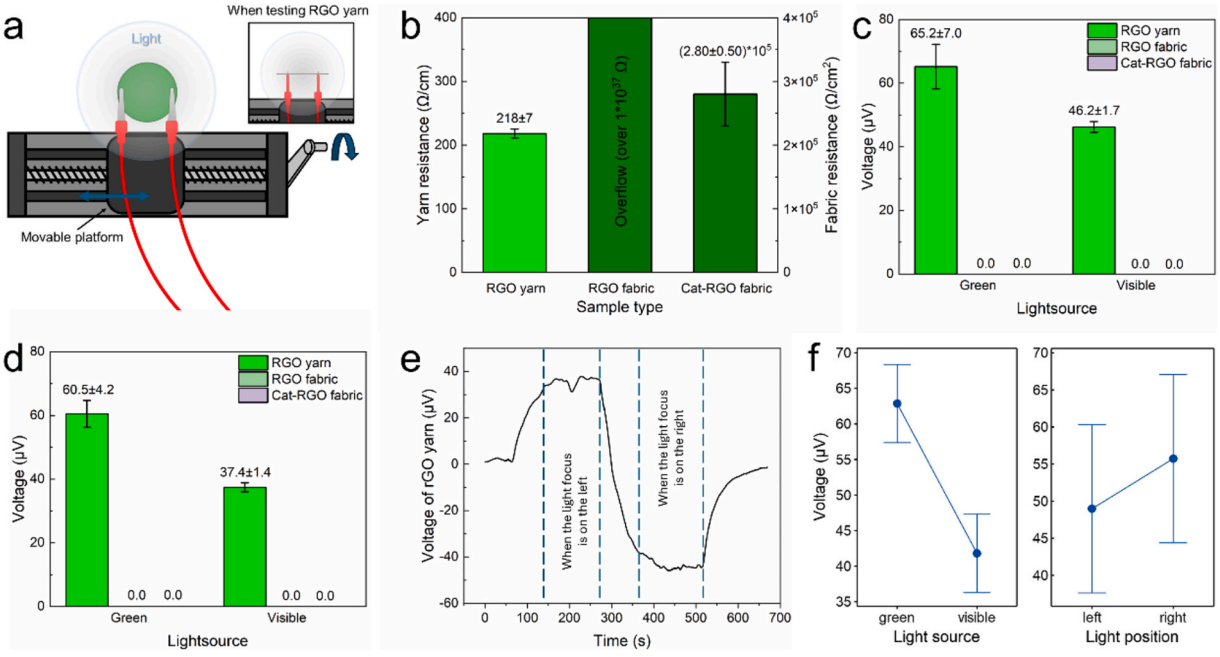

Fig. 5. The photovoltaic effect of rGO yarns and fabrics: **a)** The testing method of photovoltaic effect. **b)** The resistances of different rGO samples. **c)** The generated electromotive force of different rGO samples when the highest light irradiance is at the left side. **d)** The generated electromotive force of different rGO samples when the highest light irradiance is at the right side. **e)** The voltage changes when the light focus is on the left and right end of rGO yarn. **f)** The interval plot of voltage vs. light source and light position.

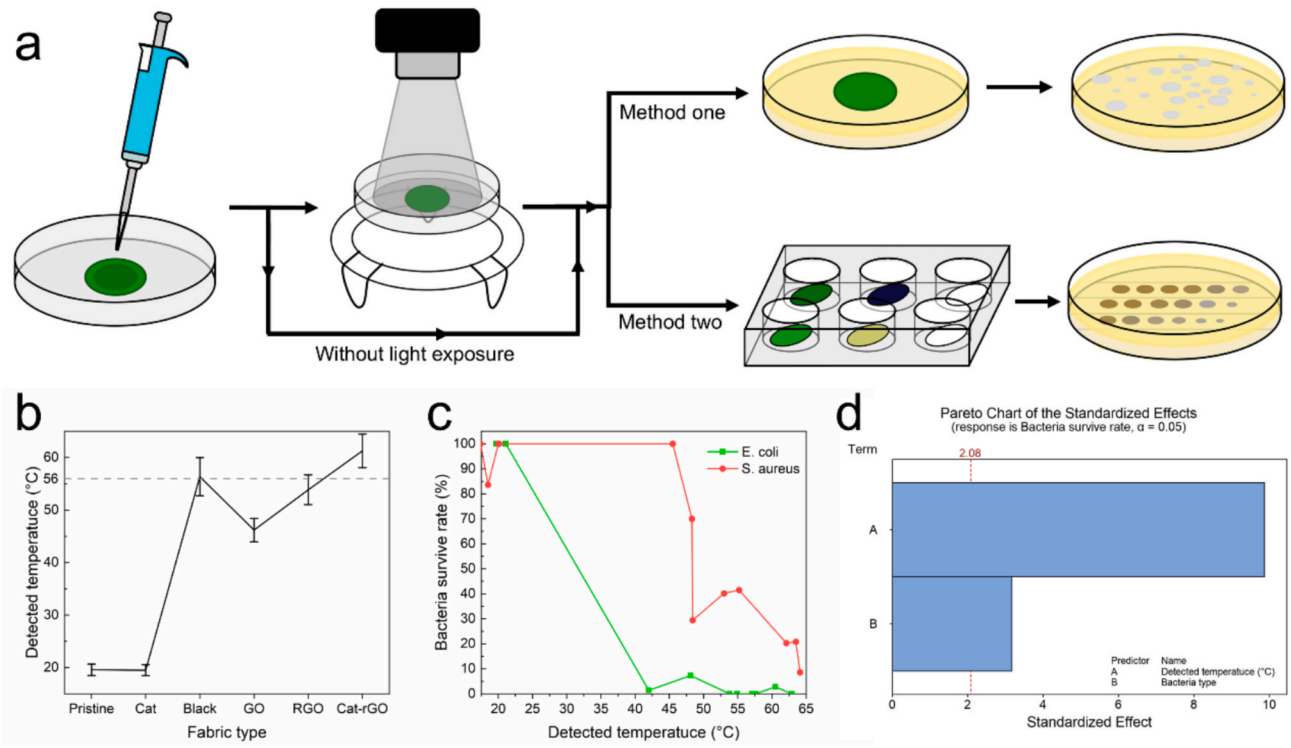

Fig. 6. **A)** The antibacterial testing procedure. **b)** The mean temperature and standard deviation of each kind of fabric under visible light exposure in a fume hood with a wind speed of 0.7 m/s. **c)** The bacteria survive rate of *S. aureus* and *E. coli* at different temperature. **d)** Pareto Chart of bacteria survive rate vs detected temperature and bacteria type.

was around 20.5 °C, and the wind speed was approximately 0.7 m/s. Under a windy condition, the detected temperature of each kind of fabric visibly decreased, as shown in Fig. 6**b**. Nevertheless, the mean temperature of the black fabric still exceeded 56 °C, and Cat-rGO fabric reached up to 61 °C.

The antibacterial performance of different fabric samples is demonstrated by their incubation results, which are displayed together with their infrared (IR) images during light exposure in Fig. 7, Fig. S10 to Fig. S12. Regarding two methods shown in Fig. 6**a,** the results of method one are corresponded to Fig. 7**a**, Fig. S10 and Fig. S11, while Fig. 7**b** and Fig. S12 correspond to the results of method two. As shown in Fig. 7**a**, Fig. S10 and Fig. S11, it is clear that under light exposure, the bacterial

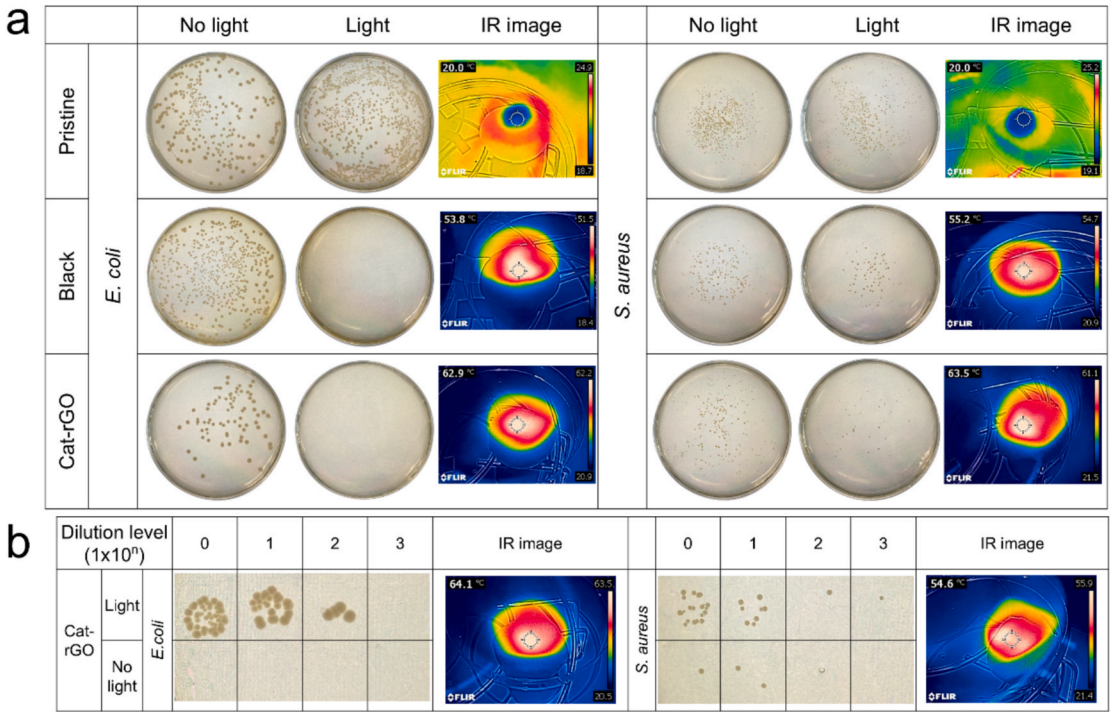

Fig. 7. **a)** The incubation results of method one. **b)** The incubation results of method two.

colonies on the pristine and Cat fabric did not decrease. Therefore, within 5 mins, CHPTAC has no significant impact on bacteria growth. Under light exposure, culture density of *E. coli* exhibits a noticeable decrease on GO fabric, and at a temperature of 48.3 °C, culture density of *S. aureus* also decreases obviously. Black, rGO, and Cat-rGO exhibited significant disinfection against *E. coli*, as only 1 or 0 colony appeared on their agar plates after the light exposure. For *S. aureus*, these three kinds of fabric also presented a noticeable inhibition to its growth, especially for black and Cat-rGO fabric when the temperature exceeded 60 °C.

To identify the impact of temperature on the bacteria, the bacteria survive rate was calculated. The survive rate is the number of colonies on the agar plate of the light-exposed fabric sample divided by the number on the agar plate of the fabric sample without light exposure. OnePetri app was used to assisting counting. When the number of colonies exceeds 500, it was recorded as 500. If the number of colonies on the agar plate of the light-exposed fabric sample is greater than the number on the agar plate of the fabric sample without light exposure, the survive rate is considered 100%. The value of the number of colonies and bacteria survive rate for each kind of fabric are listed in Table S7. In Fig. 6**c**, it is visibly that when the temperature is over 40 °C, culture density of *E. coli* sharply decreased; when temperature surpassed 52.5 °C, *E. coli* was nearly completely inactivated. As for *S. aureus*, its culture density began decreasing at 48.3 °C, and at 64.1 °C, only 8.6% of the bacteria remained.

To obtain a more accurate antibacterial performance value at high temperatures, the formula below was applied to the results in Fig. 7**b)**:

$$Antibacterial\ efficiency = \frac{X_{n1}{*}n1 - Y_{n2}{*}n2}{X_{n1}{*}n1}{*}100\% \quad (1)$$

Where X_{n1} is the number of bacteria colonies incubated from the bacteria suspension, the suspension is the one that immerses the fabric not exposed to light and is diluted n1 times, n1 is the dilution time of bacteria suspension that immerses the fabric without light exposure. Y_{n2} is the number of bacteria colonies incubated from the bacteria suspension; the suspension is the one that immerses the light exposed fabric and is diluted n2 times, n2 is the dilution time of bacterial suspension that immerses the light exposed fabric.

For *E. coli*, since the Cat-rGO fabric without light exposure had 22 bacterial colonies at dilution level 1, and the light exposed Cat-rGO fabric had no bacteria colony at dilution level 0, so the antibacterial efficiency of Cat-rGO fabric at 64.1 °C is no lower than 99%. For *S. aureus*, when the temperature is 54.6 °C, the Cat-rGO fabric without light exposure had 19 bacteria colonies at dilution level 0, while the light exposed Cat-rGO fabric had 1 bacteria colony at dilution level 0. Hence the antibacterial efficiency is about 95%.

Compared to *S. aureus*, *E. coli* is more resistant to antibiotic [77], which is due to its outer membrane containing lipopolysaccharides [78]. However, *E. coli* is more vulnerable to high temperatures than *S. aureus* [79,80]. A regression model in Minitab was used to analyse the impact of temperature and bacteria type to the bacteria survive rate, and Fig. S13 and Fig. 6**d** present the results. The results show that both temperature and bacteria type have a significant impact on the bacteria survive rate, with temperature having a greater influence than the bacteria type. The findings suggest that if the temperature is sufficiently high, both *S. aureus* and *E. coli* can be effectively inactivated. In general, Cat-rGO exhibits an obvious antibacterial performance against *S. aureus* and significant performance against *E. coli*.

4. Conclusion

To sum up, we have reported a method using cationised (Cat) cotton fabric to capture more reduced graphene oxide (rGO), and the testing results of rGO coated cotton fabric and rGO yarn in the field of photosensitive effects. The amount of rGO captured by fabric samples were demonstrated by their colours in CIELAB colour space and C/O ratio in XPS analysis. For the photothermal effect, rGO on the fabric has good light absorbance across a wide wavelength range (250–2000 nm), and the reflection rate of rGO coated cationised (Cat-rGO) fabric in this range is consistently lower than 20%. RGO's photothermal effect can be triggered by both UV and visible light, and is responsive to both narrow and broad wavelength ranges, allowing rGO coated fabrics to heat up quickly and dry quicker. Besides, rGO enhances the fabric's hydrophobicity, increasing water resistance while still allowing gradual liquid absorption. By comparison, the temperature increase of rGO yarn is far lower than that of Cat-rGO fabric. The temperature of Cat-rGO fabric can exceed 70 °C in a windless environment and 60 °C in a breezy setting under the visible light exposure, which is still high enough to kill various common viruses. Furthermore, the photothermal effect of Cat-rGO fabric is better than the heat absorption of black colour fabric. For the photovoltaic effect, Cat-rGO fabric didn't exhibit this ability, and its resistance is quite high. RGO yarn exhibited a photovoltaic effect, but the generated voltage is only at the microvolt level. Additionally, Cat-rGO fabric demonstrates good antibacterial performance against both *E. coli* and *S. aureus*. Particularly against *E. coli*, which was inactivated by over 99% within just 5 mins of light exposure, making Cat-rGO fabric a promising option for addressing antibiotic resistance in *E. coli*. Our study suggests that Cat-rGO fabric is ideal for use as RMPC, which can kill the microorganism through the light exposure, rather than using autoclaves, chemical disinfectants, or antiviral metals. This kind of self-disinfecting RMPC can be used in medical facilities, such as hospitals and nursing homes.

CRediT authorship contribution statement

Qinghong Huang: Writing – review & editing, Writing – original draft, Visualization, Methodology, Investigation, Formal analysis, Data curation. **Tianyu Kou:** Writing – review & editing, Visualization, Investigation. **Mingrui Liao:** Writing – review & editing, Methodology, Investigation, Formal analysis. **Tianhao Ge:** Writing – review & editing, Methodology, Funding acquisition, Formal analysis. **Jing Liu:** Visualization. **Jian R. Lu:** Supervision. **Heng Zhai:** Writing – review & editing, Methodology. **Yi Li:** Writing – review & editing, Supervision, Conceptualization.

Declaration of competing interest

The authors declare that they have no known competing financial interests or personal relationships that could have appeared to influence the work reported in this paper.

Acknowledgement

This work was supported by the Henry Royce Institute for Advanced Materials, funded through EPSRC grants EP/R00661X/1, EP/S019367/1, EP/P025021/1 and EP/P025498/1.

We wish to thank Hannah Rampley from University of Manchester for her help on the surface colour modification to cotton fabric.

Appendix A. Supplementary data

Supplementary data to this article can be found online at https://doi.org/10.1016/j.matdes.2025.114075.

Data availability

Data will be made available on request.

References

[1] WHO Coronavirus (COVID-19) Dashboard, 2023. https://data.who.int/dashboards/covid19/cases?n=c. (Accessed 17 Oct 2023).

[2] Technical specifications of personal protective equipment for COVID-19, 2020. https://www.who.int/publications/i/item/WHO-2019-nCoV-PPE_specifications-2020.1. (Accessed 3 March 2024).
[3] M. Liao, H. Liu, X. Wang, X. Hu, Y. Huang, X. Liu, K. Brenan, J. Mecha, M. Nirmalan, J.R. Lu, A technical review of face mask wearing in preventing respiratory COVID-19 transmission, Curr. Opin. Colloid Interface Sci. 52 (2021) 101417.
[4] Learn About Aquatic Trash, 2023. https://www.epa.gov/trash-free-waters/learn-about-aquatic-trash. (Accessed 2 March 2024).
[5] M.B. Gill, K.L. Jensen, D.M. Lambert, S. Upendram, B.C. English, N. Labbé, S. W. Jackson, R.J. Menard, Consumer preferences for eco-friendly attributes in disposable dinnerware, Resour. Conserv. Recycl. 161 (2020).
[6] M.T. Khan, I.A. Shah, M.F. Hossain, N. Akther, Y. Zhou, M.S. Khan, M. Al-Shaeli, M. S. Bacha, I. Ihsanullah, Personal protective equipment (PPE) disposal during COVID-19: an emerging source of microplastic and microfiber pollution in the environment, Sci. Total Environ. 860 (2023) 160322.
[7] E. Vozzola, M. Overcash, E. Griffing, Environmental considerations in the selection of isolation gowns: a life cycle assessment of reusable and disposable alternatives, Am. J. Infect. Control 46 (8) (2018) 881–886.
[8] Z. Sun, X. Cai, C. Gu, R. Zhang, W. Han, Y. Qian, Y. Wang, W. Xu, Y. Wu, X. Cheng, Z. Yuan, Y. Xie, D. Qu, Survival of SARS-COV-2 under liquid medium, dry filter paper and acidic conditions, Cell Discovery 6 (1) (2020) 57.
[9] J. Reissner, P. Siller, A. Bartel, U. Roesler, A. Friese, Stability of Feline Coronavirus in aerosols and dried in organic matrices on surfaces at various environmental conditions, Sci. Rep. 13 (1) (2023) 22012.
[10] Why do viruses survive outside the human body?, 2020. https://covid19.nj.gov/faqs/coronavirus-information/about-the-virus/why-do-viruses-survive-outside-the-human-body#direct-link. (Accessed 3 June 2024).
[11] H.F. Rabenau, J. Cinatl, B. Morgenstern, G. Bauer, W. Preiser, H.W. Doerr, Stability and inactivation of SARS coronavirus, Med. Microbiol. Immunol. 194 (1–2) (2005) 1–6.
[12] M.T. Brady, J. Evans, J. Cuartas, Survival and disinfection of parainfluenza viruses on environmental surfaces, Am. J. Infect. Control 18 (1) (1990) 18–23.
[13] R. Fischer, S. Judson, K. Miazgowicz, T. Bushmaker, J. Prescott, V. Munster, Ebola virus stability on surfaces and in fluids in simulated outbreak environments, Emerg. Infect. Dis. 21 (7) (2015) 1243.
[14] S.B. Tamrakar, J. Henley, P.L. Gurian, C.P. Gerba, J. Mitchell, K. Enger, J.B. Rose, Persistence analysis of poliovirus on three different types of fomites, J. Appl. Microbiol. 122 (2) (2017) 522–530.
[15] B. Bean, B.M. Moore, B. Sterner, L.R. Peterson, D.N. Gerding, H.H. Balfour Jr., Survival of influenza viruses on environmental surfaces, J Infect Dis 146 (1) (1982) 47–51.
[16] C.K. Yinda, D. Morris, R. Fischer, S. Gallogly, Z. Weishampel, J. Port, T. Bushmaker, J. Schulz, K. Bibby, N. van Doremalen, J. Lloyd-Smith, V. Munster, Stability of Monkeypox virus in body fluids and wastewater, Emerg. Infect. Dis. 29 (10) (2023) 2065.
[17] J. Archer, A. Mikelonis, B. Wyrzykowska-Ceradini, E. Morris, J. Sawyer, T. Chamberlain, A. Abdel-Hady, M. Monge, A. Touati, Evaluation of disinfection methods for personal protective equipment (PPE) items for reuse during a pandemic, PLoS One 18 (7) (2023) e0287664.
[18] Disinfection and Reuse of Personal Protective Equipment, 2022. https://www.dhs.gov/publication/st-disinfection-and-reuse-personal-protective-equipment. (Accessed 3 March 2024).
[19] S. Beikzadeh, A. Akbarinejad, J. Taylor, J. Perera, J. Ross, S. Swift, P.A. Kilmartin, J. Travas-Sejdic, From energy storage to pathogen eradication: unveiling the antibacterial and antiviral capacities of flexible solid-state carbon cloth supercapacitors, J. Mater. Chem. B 11 (34) (2023) 8170–8181.
[20] C. Liu, X. Xie, W. Zhao, J. Yao, D. Kong, A.B. Boehm, Y. Cui, Static electricity powered copper oxide nanowire microbicidal electroporation for water disinfection, Nano Lett. 14 (10) (2014) 5603–5608.
[21] A.M. Nair, A. Kumar, N.H. Barbhuiya, S.P. Singh, Electrochemical inactivation of enteric viruses MS2, T4, and Phi6 using doped laser-induced graphene electrodes and filters, Environ. Sci. Nano 10 (8) (2023) 2077–2089.
[22] Z.Y. Huo, Y.J. Kim, I.Y. Suh, D.M. Lee, J.H. Lee, Y. Du, S. Wang, H.J. Yoon, S. W. Kim, Triboelectrification induced self-powered microbial disinfection using nanowire-enhanced localized electric field, Nat. Commun. 12 (1) (2021) 3693.
[23] X. Ren, J. Liang, Smart anti-microbial composite coatings for textiles and plastics, in: M.M. Fatima (Ed.), Smart Composite Coatings and Membranes, Woodhead Publishing, Cambridge, 2016, pp. 235–259.
[24] L. Li, D. Chen, J. Chen, C. Yang, Y. Zeng, T. Jin, Y. Zhang, X. Sun, H. Mao, Z. Mu, X. Shen, Z. Ruan, X. Cai, Gelatin and catechol-modified quaternary chitosan cotton dressings with rapid hemostasis and high-efficiency antimicrobial capacity to manage severe bleeding wounds, Mater. Des. 229 (2023).
[25] S. Karagoz, N.B. Kiremitler, G. Sarp, S. Pekdemir, S. Salem, A.G. Goksu, M.S. Onses, I. Sozdutmaz, E. Sahmetlioglu, E.S. Ozkara, A. Ceylan, E. Yilmaz, Antibacterial, antiviral, and self-cleaning mats with sensing capabilities based on electrospun nanofibers decorated with ZnO nanorods and Ag nanoparticles for protective clothing applications, ACS Appl. Mater. Interfaces 13 (4) (2021) 5678–5690.
[26] Q. Huang, C. Meng, M. Liao, T. Kou, F. Zhou, J.R. Lu, J. Li, Y. Li, Hierarchically porous, superhydrophobic PLLA/copper composite fibrous membranes for air filtration, ACS Appl. Polym. Mater. 6 (4) (2024) 2381–2391.
[27] M. Qu, Z. Luo, H. Chen, Y. Qin, D.W. Schubert, G. Yang, L. Han, F. Nilsson, Strain sensing, electromagnetic interference shielding, and antimicrobial performance of triple hierarchic fabric coated with AgNWs and polydopamine, Mater. Des. 243 (2024).
[28] Z.U. Iyigundogdu, O. Demir, A.B. Asutay, F. Sahin, Developing novel antimicrobial and antiviral textile products, Appl. Biochem. Biotechnol. 181 (3) (2017) 1155–1166.
[29] R. Gulati, S. Sharma, R.K. Sharma, Antimicrobial textile: recent developments and functional perspective, Polym. Bull. (Berl) 79 (8) (2022) 5747–5771.
[30] M.E. Darnell, K. Subbarao, S.M. Feinstone, D.R. Taylor, Inactivation of the coronavirus that induces severe acute respiratory syndrome, SARS-CoV, J. Virol. Methods 121 (1) (2004) 85–91.
[31] C. Batejat, Q. Grassin, J.C. Manuguerra, I. Leclercq, Heat inactivation of the severe acute respiratory syndrome coronavirus 2, J. Biosafety Biosecurity 3 (1) (2021) 1–3.
[32] I. Béládi, I. Mucsi, M. Bakay, R. Pusztai, Rescue of heat-inactivated adenovirus type 1 and 6 by ultraviolet-irradiated adenovirus type 8, J. Gen. Virol. 7 (2) (1970) 153–158.
[33] N.E. Babady, Y.-W. Tang, Respiratory Syncytial Virus and Human Metapneumovirus, in: J.H. Jorgensen, K.C. Carroll, G. Funke, M.A. Pfaller, M. L. Landry, S.S. Richter, D.W. Warnock (Eds.), Manual of Clinical Microbiology, ASM Press, Washington, D.C., 2015, pp. 1498–1518.
[34] M. Arita, M. Matsumoto, Heat inactivation of measles virus, Jpn. J. Microbiol. 12 (1) (1968) 121–122.
[35] Information on the Survivability of the Ebolavirus in Medical Waste, 2023. https://www.cdc.gov/vhf/ebola/clinicians/cleaning/ebola-virus-survivability.html. (Accessed 30 Oct 2023).
[36] A. Norman, R.C. Veomett, Heat inactivation of poliovirus ribonucleic acid, Virology 12 (1) (1960) 136–139.
[37] S. Zou, J. Guo, R. Gao, L. Dong, J. Zhou, Y. Zhang, J. Dong, H. Bo, K. Qin, Y. Shu, Inactivation of the novel avian influenza A (H7N9) virus under physical conditions or chemical agents treatment, J. Virol. 10 (1) (2013) 289.
[38] D. Mariotti, A. Bettini, S. Meschi, S. Notari, M. Francalancia, E. Tartaglia, D. Lapa, E. Specchiarello, E. Girardi, G. Matusali, F. Maggi, Effect of chemical and physical agents on monkeypox virus infectivity and downstream research applications, Virology 592 (2024) 109993.
[39] D.S. Leland, Parainfluenza and Mumps Viruses, in: J.H. Jorgensen, K.C. Carroll, G. Funke, M.A. Pfaller, M.L. Landry, S.S. Richter, D.W. Warnock (Eds.), Manual of Clinical Microbiology, ASM Press, Washington, DC, 2015, pp. 1487–1497.
[40] K.J. Henrickson, Parainfluenza viruses, Clin. Microbiol. Rev. 16 (2) (2003) 242–264.
[41] L. Huang, S. Xu, Z. Wang, K. Xue, J. Su, Y. Song, S. Chen, C. Zhu, B.Z. Tang, R. Ye, Self-reporting and photothermally enhanced rapid bacterial killing on a laser-induced graphene mask, ACS Nano 14 (9) (2020) 12045–12053.
[42] H. Zhong, Z. Zhu, J. Lin, C.F. Cheung, V.L. Lu, F. Yan, C.Y. Chan, G. Li, Reusable and recyclable graphene masks with outstanding superhydrophobic and photothermal performances, ACS Nano 14 (5) (2020) 6213–6221.
[43] S. Ye, K. Shao, Z. Li, N. Guo, Y. Zuo, Q. Li, Z. Lu, L. Chen, Q. He, H. Han, Antiviral activity of graphene oxide: how sharp edged structure and charge matter, ACS Appl. Mater. Interfaces 7 (38) (2015) 21571–21579.
[44] J. Ren, C. Wang, X. Zhang, T. Carey, K. Chen, Y. Yin, F. Torrisi, Environmentally-friendly conductive cotton fabric as flexible strain sensor based on hot press reduced graphene oxide, Carbon 111 (2017) 622–630.
[45] S. Bhattacharjee, R. Joshi, A.A. Chughtai, C.R. Macintyre, Graphene modified multifunctional personal protective clothing, Adv. Mater. Interfaces 6 (21) (2019) 1900622.
[46] T. Seifi, A. Reza Kamali, Antiviral performance of graphene-based materials with emphasis on COVID-19: a review, Med. Drug Discov. 11 (2021) 100099.
[47] H.E. Karahan, Y. Wang, W. Li, F. Liu, L. Wang, X. Sui, M.A. Riaz, Y. Chen, Antimicrobial graphene materials: the interplay of complex materials characteristics and competing mechanisms, Biomater. Sci. 6 (4) (2018) 766–773.
[48] H. Cheraghi Bidsorkhi, N. Faramarzi, B. Ali, L.R. Ballam, A.G. D'Aloia, A. Tamburrano, M.S. Sarto, Wearable graphene-based smart face mask for real-time human respiration monitoring, Mater. Des. 230 (2023) 111970.
[49] C. Li, R. Ye, J. Bouckaert, A. Zurutuza, D. Drider, T. Dumych, S. Paryzhak, V. Vovk, R.O. Bilyy, S. Melinte, M. Li, R. Boukherroub, S. Szunerits, Flexible nanoholey patches for antibiotic-free treatments of skin infections, ACS Appl. Mater. Interfaces 9 (42) (2017) 36665–36674.
[50] G. Cai, Z. Xu, M. Yang, B. Tang, X. Wang, Functionalization of cotton fabrics through thermal reduction of graphene oxide, Appl. Surf. Sci. 393 (2017) 441–448.
[51] Y. Liu, L. Xia, Q. Zhang, H. Guo, A. Wang, W. Xu, Y. Wang, Structure and properties of carboxymethyl cotton fabric loaded by reduced graphene oxide, Carbohydr. Polym. 214 (2019) 117–123.
[52] Y. Zhao, Y. Meng, P. Yu, X. Hu, J. Su, J. Han, Modified reduced graphene oxide-LDH/WPU nanohybrid coated nylon 6 fabrics for durable photothermal conversion performance, Appl. Surf. Sci. 622 (2023).
[53] I.A. Sahito, K.C. Sun, A.A. Arbab, M.B. Qadir, Y.S. Choi, S.H. Jeong, Flexible and conductive cotton fabric counter electrode coated with graphene nanosheets for high efficiency dye sensitized solar cell, J. Power Sources 319 (2016) 90–98.
[54] Y. Tu, W. Tang, L. Yu, Z. Liu, Y. Liu, H. Xia, H. Zhang, S. Chen, J. Wu, X. Cui, J. Zhang, F. Wang, Y. Hu, D. Deng, Inactivating SARS-CoV-2 by electrochemical oxidation, Sci. Bull. 66 (7) (2021) 720–726.
[55] C. Yang, L. Wen, Y. Li, X.-Y. Li, Fabrication of SnO_2-Sb reactive membrane electrodes for high-efficiency electrochemical inactivation of bacteria and viruses in water, Chem. Eng. J. 446 (2022).
[56] N. Karim, S. Afroj, S. Tan, P. He, A. Fernando, C. Carr, K.S. Novoselov, Scalable production of graphene-based wearable E-textiles, ACS Nano 11 (12) (2017) 12266–12275.

[57] L. Xu, Z. Liu, H. Zhai, X. Chen, R. Sun, S. Lyu, Y. Fan, Y. Yi, Z. Chen, L. Jin, J. Zhang, Y. Li, T.T. Ye, Moisture-resilient graphene-dyed wool fabric for strain sensing, ACS Appl. Mater. Interfaces 12 (11) (2020) 13265–13274.
[58] J. Correia, K.T. Rainert, F.R. Oliveira, R. de Cássia Siqueira Curto Valle, J.A. B. Valle, Cationization of cotton fiber: an integrated view of cationic agents, processes variables, properties, market and future prospects, Cellulose 27 (15) (2020) 8527–8550.
[59] S. Zhai, Y. Li, W. Dong, H. Zhao, K. Ma, H. Zhang, H. Wang, Y. Zhao, X. Li, Z. Cai, Cationic cotton modified by 3-chloro-2-hydroxypropyl trimethyl ammonium chloride for salt-free dyeing with high levelling performance, Cellulose 29 (1) (2021) 633–646.
[60] A. Nallathambi, G.D. Venkateshwarapuram Rengaswami, Salt-free reactive dyeing of cotton hosiery fabrics by exhaust application of cationic agent, Carbohydr. Polym. 152 (2016) 1–11.
[61] M. Hasani, M. Montazer, Cationization of cellulose/polyamide on UV protection, bio-activity, and electro-conductivity of graphene oxide-treated fabric, J. Appl. Polym. Sci. 134 (44) (2017).
[62] I.A. Sahito, K.C. Sun, A.A. Arbab, M.B. Qadir, S.H. Jeong, Integrating high electrical conductivity and photocatalytic activity in cotton fabric by cationizing for enriched coating of negatively charged graphene oxide, Carbohydr. Polym. 130 (2015) 299–306.
[63] Z. Xu, H. Sun, X. Zhao, C. Gao, Ultrastrong fibers assembled from giant graphene oxide sheets, Adv. Mater. 25 (2) (2013) 188–193.
[64] H. Zhai, L. Xu, Z. Liu, L. Jin, Y. Yi, J. Zhang, Y. Fan, D. Cheng, J. Li, X. Liu, Q. Song, P. Yue, Y. Li, Twisted graphene fibre based breathable, wettable and washable anti-jamming strain sensor for underwater motion sensing, Chem. Eng. J. 439 (2022).
[65] K.K.H. De Silva, H.-H. Huang, M. Yoshimura, Progress of reduction of graphene oxide by ascorbic acid, Appl. Surf. Sci. 447 (2018) 338–346.
[66] S. Joshi, R. Siddiqui, P. Sharma, R. Kumar, G. Verma, A. Saini, Green synthesis of peptide functionalized reduced graphene oxide (rGO) nano bioconjugate with enhanced antibacterial activity, Sci. Rep. 10 (1) (2020) 9441.
[67] S. Stankovich, D.A. Dikin, R.D. Piner, K.A. Kohlhaas, A. Kleinhammes, Y. Jia, Y. Wu, S.T. Nguyen, R.S. Ruoff, Synthesis of graphene-based nanosheets via chemical reduction of exfoliated graphite oxide, Carbon 45 (7) (2007) 1558–1565.
[68] Q.-H. Huang, Z.-C. Liu, T.J.L. Null, Y. Li, Influence of fabric structure and properties on thermal comfort of medical protective clothing, J. Fiber Bioeng. Inf. 15 (4) (2022) 259–274.
[69] J. Zhang, H. Yang, G. Shen, P. Cheng, J. Zhang, S. Guo, Reduction of graphene oxide via L-ascorbic acid, Chem. Commun. 46 (7) (2010) 1112–1114.
[70] M.S. Dresselhaus, A. Jorio, A.G. Souza Filho, R. Saito, Defect characterization in graphene and carbon nanotubes using Raman spectroscopy, Philos. Trans. R. Soc. A 368 (1932) (2010) 5355–5377.
[71] M. Bruna, A.K. Ott, M. Ijäs, D. Yoon, U. Sassi, A.C. Ferrari, Doping dependence of the Raman spectrum of defected graphene, ACS Nano 8 (7) (2014) 7432–7441.
[72] M.D. Bhatt, H. Kim, G. Kim, Various defects in graphene: a review, RSC Adv. 12 (33) (2022) 21520–21547.
[73] T. Topalovic, V.A. Nierstrasz, L. Bautista, D. Jocic, A. Navarro, M.M.C. G. Warmoeskerken, XPS and contact angle study of cotton surface oxidation by catalytic bleaching, Colloids Surf. A Physicochem. Eng. Asp. 296 (1–3) (2007) 76–85.
[74] R. Rozada, J.I. Paredes, M.J. Lopez, S. Villar-Rodil, I. Cabria, J.A. Alonso, A. Martinez-Alonso, J.M. Tascon, From graphene oxide to pristine graphene: revealing the inner workings of the full structural restoration, Nanoscale 7 (6) (2015) 2374–2390.
[75] J. Lee, H.-R. Chae, Y.J. Won, K. Lee, C.-H. Lee, H.H. Lee, I.-C. Kim, J.-M. Lee, Graphene oxide nanoplatelets composite membrane with hydrophilic and antifouling properties for wastewater treatment, J. Membr. Sci. 448 (2013) 223–230.
[76] L. Dashairya, M. Rout, P. Saha, Reduced graphene oxide-coated cotton as an efficient absorbent in oil-water separation, Adv. Compos. Mater. 1 (1) (2017) 135–148.
[77] H. Gong, M. Liao, X. Hu, K. Fa, S. Phanphak, D. Ciumac, P. Hollowell, K. Shen, L. A. Clifton, M. Campana, J.R.P. Webster, G. Fragneto, T.A. Waigh, A.J. McBain, J. R. Lu, Aggregated amphiphilic antimicrobial peptides embedded in bacterial membranes, ACS Appl. Mater. Interfaces 12 (40) (2020) 44420–44432.
[78] M. Liao, H. Gong, X. Quan, Z. Wang, X. Hu, Z. Chen, Z. Li, H. Liu, L. Zhang, A. J. McBain, T.A. Waigh, J. Zhou, J.R. Lu, Intramembrane nanoaggregates of antimicrobial peptides play a vital role in bacterial killing, Small 19 (3) (2023) e2204428.
[79] S.C. Stringer, S.M. George, M.W. Peck, Thermal inactivation of Escherichia coli O157:H7, Symp. Ser. Soc. Appl. Microbiol. (29) (2000) 79S–89S.
[80] J. Kennedy, I.S. Blair, D.A. McDowell, D.J. Bolton, An investigation of the thermal inactivation of Staphylococcus aureus and the potential for increased thermotolerance as a result of chilled storage, J. Appl. Microbiol. 99 (5) (2005) 1229–1235.